Solid Freeform Fabrication 2022: Proceedings of the 33rd Annual International Solid Freeform Fabrication Symposium – An Additive Manufacturing Conference
Reviewed Paper

Investigating the influence of thermal and mechanical properties of resin on the sedimentation rate of the printed geometry in the volumetric additive manufacturing technique

Roozbeh Salajeghe*, Carl Sander Kruse*, Daniel Helmuth Meile*, Deepak Marla†, and Jon Spangenberg*

* Department of Mechanical Engineering, Technical University of Denmark, 2800 Kgs. Lyngby, Denmark
†Department of Mechanical Engineering, India Institute of Technology Bombay, Mumbai, India

Abstract

Converse to the conventional additive manufacturing methods based on constructing a body layer by layer, volumetric additive manufacturing produces the whole geometry at the same time. While it is faster, creates features with high surface quality, requires no overhang support structures, and can print in high-viscosity resins, all of which push the limits of additive manufacturing, this technique is still premature and suffers from some effects such as body sedimentation that impacts the geometric fidelity and resolution of the final product. The sedimentation rate of the printed body during its formation is highly dependent on the resin type, its viscosity, and its curing behavior. Herein, we propose a CFD model that takes into account the synergistic effect of reaction-based heating, curing behavior, and resin properties to predict the sedimentation rate of the printed geometry. The results show that heating effects can slow down the sedimentation rate of the curing part significantly.

Keywords: Volumetric additive manufacturing, Volume of Fluid, Sedimentation, Boussinesq approximation, ultra-violet (UV) Curing, Photopolymerization

Introduction

****

Volumetric additive manufacturing (VAM) is a new additive manufacturing method developed by Kelly et al. [1], which prints the whole volume of the geometry at the same time unlike conventional methods that function in a layer-by-layer manner. VAM offers higher printing rates, no requirement of a support for overhanging parts, and applicability to high viscosities, which are the shortcomings of the conventional additive manufacturing methods [2]. In VAM, a cylindrical container that rotates at a constant rotational velocity encompasses the photosensitive resin. An algorithm that is based on the tomographic reconstruction method takes predefined geometries and converts them into modulated intensity profiles. A projector illuminates these intensity profiles into the cylindrical container, synchronized with its rotation rate so that the accumulated energy dose inside the printing domain matches the desired geometry. The photosensitive resin contains some inhibitors, such as molecular oxygen for acrylates, which prevent the photocuring process. Thanks to the inhibition effect, the polymerization would not occur at the very first instant when the resin receives light, which makes the VAM process feasible [2]. The curing of the resin would start where and when the accumulated light energy dose goes above a threshold for which the inhibitors are depleted locally. Accordingly, it is very important that the VAM algorithm modulates the intensity in a way that the built-up intensity in the desired locations reaches the threshold at the same time. Otherwise, one part of the geometry would cure faster than the others. The cured part would start to sink down due to its higher density which prevents the formation of the geometry. The schematic of the geometry is shown in Figure 1.

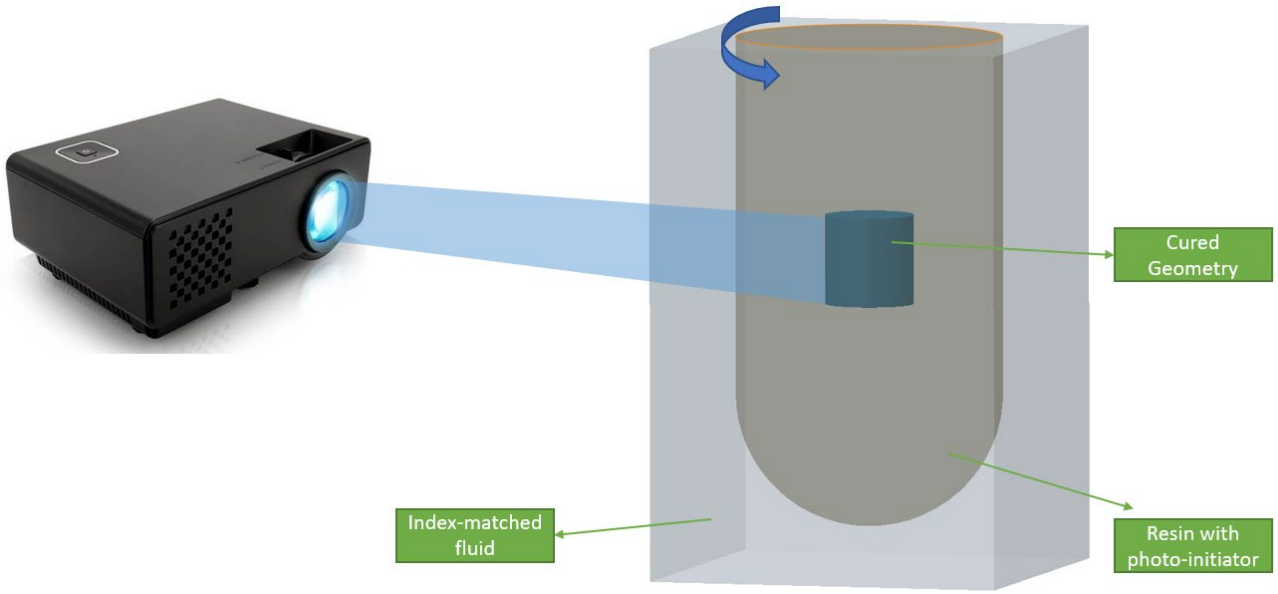

Figure 1: The schematic of the principles of the VAM technique. The tube containing the photo-curable resin and the photo-initiator rotates inside a container with index-matched fluid.

Kelly et al. pioneered in the field of VAM by introducing its working principles and its computed tomographic algorithm and presenting the specifications of the 3d geometries they produce with this method [1]. Later, they used the VAM method to print complex, sub-centimeter scale geometries with different materials, including acrylate polymers and hydrogels, in a time span between 30 and 300 seconds [2]. They further explained the underlying physics of the method and formulated the effect of some optical parameters and properties of the resin on the VAM printing time. By applying the VAM method to the printing of complex geometries, Loterie et al. improved the method by enhancing its resolution and diminishing the printing time to less than 30 seconds [3,4]. Orth et al. [5] suggested some corrections in the VAM algorithm to computationally account for the beam lensing effect and its non-telecentricity. Rackson et al. [6] showed that introducing a uniform illumination at the end of the projection period will not only mitigate some surface defects known as striations but also increase the possibility of simultaneous part formation, mitigating its premature sedimentation. In another study [7], they proposed a new projection algorithm that increases the contrast between the built-up light intensity of the target region of the resin and its surrounding, leading to more accuracy and higher geometric fidelity of the printed part. Wang et al. [8] used two different projection wavelengths to create structures with gradient in their mechanical properties. Some researchers applied the VAM method to other materials. Cook et al. [9] formulated thiolene resins, which are printable with the VAM method and managed to create structures with diverse mechanical properties. Using preceramic polymer resins, Kollep et al. [10] applied the VAM method to build ceramics. Wolff et al. [11] further extended the VAM applicability to scattering resins.

Despite all the benefits of VAM, this method still suffers from some issues, such as premature sedimentation, in which the printed part starts to sediment before it is fully formed. The sedimentation phenomenon adversely affects the geometric fidelity and resolution of the printed part, and in some cases, it even prevents its formation. Kelly et al. tried to derive an analytical formulation for the sedimentation rate of a simple spheroid by considering the Stokes drag applied to the geometry [2]; however, the model's predictions were much higher than the experimental results. Letorie el al. observed that the oval-shaped VAM-printed geometry does not sink until 20 seconds after the end of the print time [4], and Rackson et al. reported that sedimentation could be so intense that it can even

disturb part formation [6,12]. Kollep et al observed that their part slightly moves upwards during the print time while it gradually starts to sink after the projector turn-off [10].

Herein, the different and sometimes strange behaviors of the printed parts during and after the projection are attributed to the thermal effects and how the mechanical and thermal properties of the materials react to those effects. To substantiate our hypothesis, we present a simple numerical model taking into account thermal effects and their influence on mechanical properties. Numerical models have shown to be very potent when it comes to predicting the results and elucidating the underlying physics. In the field of additive manufacturing, many studies have been done to model and improve the metal [13–15] and polymer [16–20] 3D printing. Here, we present the first numerical model for the subject of the VAM method, which is a sub-category of polymer additive manufacturing.

Methodology

****

The physics of the problem is modeled using the VOF method by considering the uncured phase as the 1st phase and the curing phase as the 2nd phase. On top of the two-phase Navier-Stokes equations, an energy equation is also solved to obtain the temperature field, which is then used to modify the density of the fluid. To make the model simple, the temperature-based variation of the fluid density is implemented according to the Boussinesq approximation, in which the change in density is only made in the gravity force. The governing equations are as follows [21,22].

$$\nabla . U = 0 \tag{1}$$

$$\frac{\partial(\rho \mathrm{U})}{\partial \mathrm{t}} + \nabla .(\rho UU) - \nabla .(\mu \nabla U) - (\nabla U).\nabla \mu = -\nabla \mathrm{p_d} - g.x\nabla \rho_k + \sigma \kappa \nabla \alpha \tag{2}$$

$$\frac{\partial \alpha}{\partial \mathrm{t}} + \nabla .(U\alpha) + \nabla .[U_r \alpha(1-\alpha)] = 0 \tag{3}$$

$$\rho = \rho_1 \alpha + \rho_2(1-\alpha) \tag{4}$$

$$\mu = \mu_1 \alpha + \mu_2(1-\alpha) \tag{5}$$

$$\kappa = -\nabla .(\frac{\nabla \alpha}{|\nabla \alpha|}) \tag{6}$$

$$\rho_k = \rho(1-\beta(T-T_0)) \tag{7}$$

$$p_d = p - \rho g.x \tag{8}$$

$$\frac{\partial(\rho \mathrm{T})}{\partial \mathrm{t}} + \nabla .(\rho UT) = \nabla .\left(\frac{k}{c_p}\nabla \mathrm{T}\right) + \frac{q_v}{c_p} \tag{9}$$

In Eqs. ((1)-(9)), U is the velocity vector, p is the pressure, T is the temperature, and α is the phase indicator variable which takes the value of 0 for one phase, and 1 for the other phase. The set of partial differential equation introduced in Eqs. ((1)-(9)) are solved using OpenFOAM. Other parameters and variables are defined below.

Table 1: parameters and variables used in this simulation

Parameter/Variable	Definition	Formulation	Value (if applicable)
T_0	Reference temperature	-	$300\ K$
ρ_1	Density of the uncured phase	-	$1100\ kg/m^3$
ρ_2	Density of the curing phase	-	$1210\ kg/m^3$

ρ	Mixture density	Eq. (4)	-
ρ_k	Boussinesq density	-	-
μ_1	Viscosity of the uncured phase	-	5 $Pa.s$
μ_2	Viscosity of the curing phase	-	5 $Pa.s$
μ	Mixture viscosity	Eq. (5)	5 $Pa.s$
$\mathrm{p_d}$	Modified pressure	Eq. (8)	-
g	Gravitational acceleration	-	(0, 0, -9.81) m/s^2
x	Position vector	-	-
κ	Interface curvature	Eq. (6)	-
U_r	Relative velocity between the phases in the interface	-	-
β	Coefficient of thermal expansion	-	0.001 $1/K$
k	Thermal conductivity	-	0.142 W/mK
c_p	Specific heat	-	1500 J/kgK
q_v	Heat generation per unit volume	-	5 $kcal/mol$ per acrylate double bond

The values for densities (ρ_1 and ρ_2) and viscosities (μ_1 and μ_2) are based on a 3:1 BPAGDA:PEGDA ratio mixture according to reference [2]. The thermal properties are considered to be equal for both phases and are taken close to the ones that are reported in reference [23]. For the heat generation, the value that is reported in reference [23] is $20.6\ kcal/mol$ for the complete polymerization process with high enough intensity. However, as only a ratio of the photopolymerization process takes place in the VAM and the intensities might be lower than the one for which the value of heat generation is reported, here, a value of $5\ \mathrm{kcal/mol}$ is used, which is approximately one-fifth of the value reported in [23]. The heat source is only active where the curing phase exists. It means that it moves with the movement of the second phase.

The computational domain along with the boundary and initial conditions is shown in Figure 2. The printed part is considered to be a simple cylinder that deforms because of the shear-induced forces that are exerted on it when it moves down.

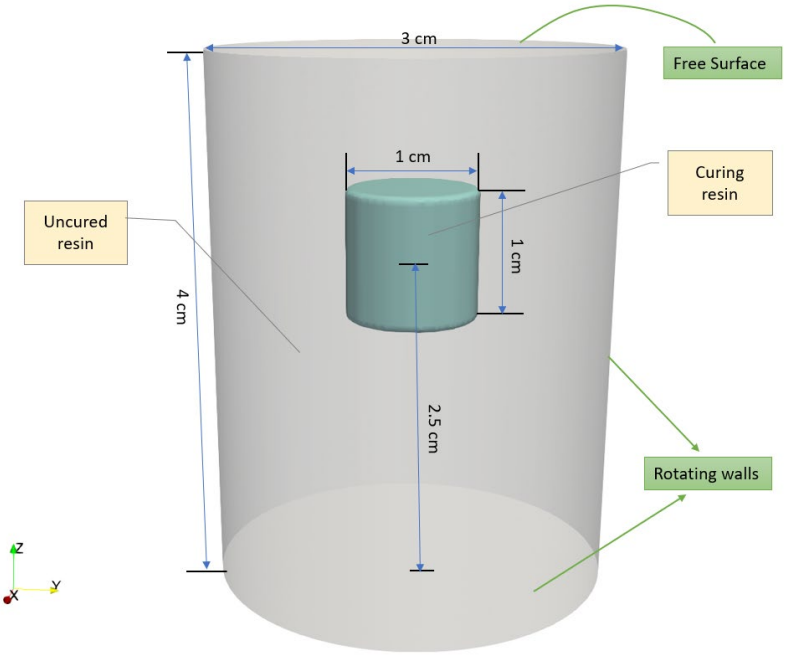

Figure 2: The computational domain, boundary and initial conditions

Results and discussions

****

Figure 3 shows the phase indicator field (top row) and temperature field (bottom row) at t=2 s (left column), t=4s (middle column), and t=6s (right column). The viscosity of the curing phase is set equal to the surrounding uncured resin so that the deformations are shown with exaggeration. From this figure, it is clear how the curing phase sinks down because of its higher density compared to the surrounding fluid. In sub-figures (d-f), the temperature field is depicted. As discussed in the previous section, the heat source is active only in the curing phase to mimic the exothermic reactions that are happening inside it. Because of the low conductivity of the material, only the near vicinity of the curing phase sense the thermal effects, and for the other parts of the resin, it takes a long time until they are influenced by the heat source.

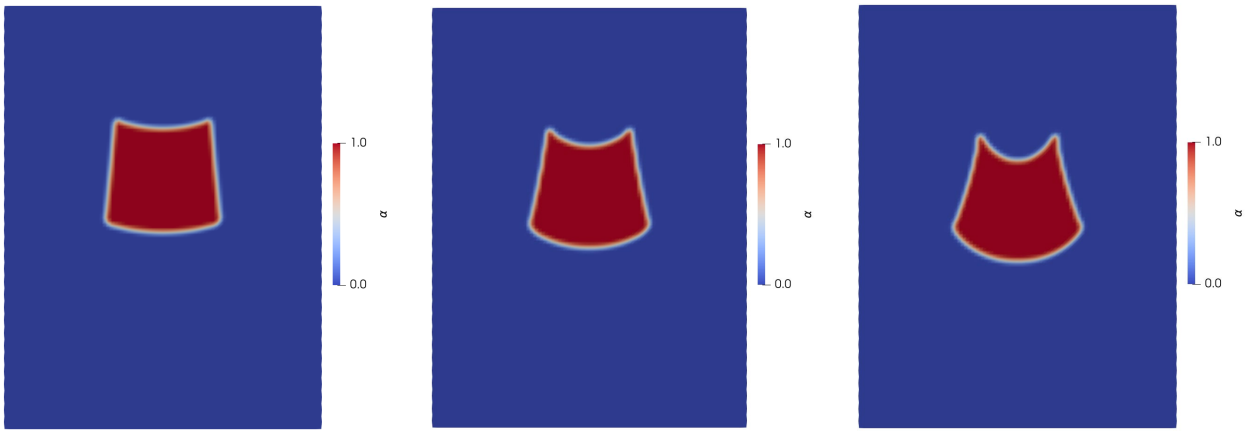

(a) α field, t=2 s (b) α field, t=4 s (c) α field, t=6 s

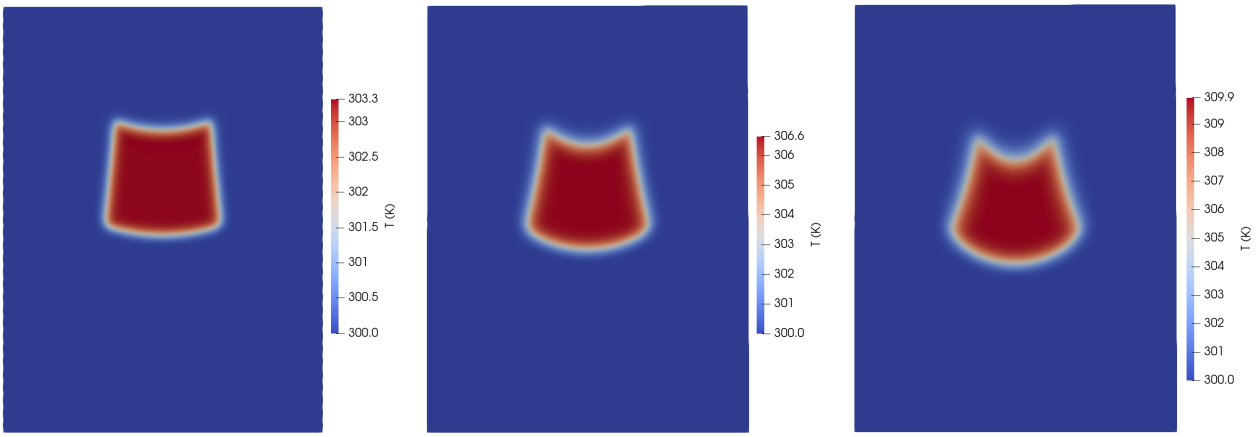

(d) temperature field, t=2 s (e) temperature field, t=4 s (f) temperature field, t=6 s

Figure 3: phase indicator variable for sub-figures (a), (b), and (c), and temperature field for sub-figures (d), (e), and (f).

Figure 4 compares the change in the vertical position of the printed part's center of gravity for two cases with and without heating effects. This figure clearly shows how the temperature increase inside the curing phase influences its density which in turn impacts the gravitational force exerted on the part and its sedimentation rate. Furthermore, it can be seen that as the temperature builds up inside the curing part, the difference between the graphs is also increased.

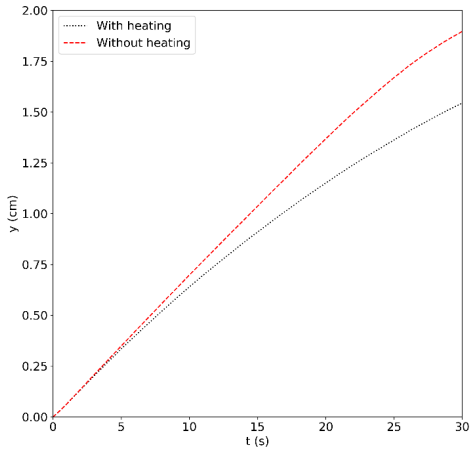

Figure 4: Variation in the center of gravity of the printed part in the vertical direction with and without heating effects

If the heating rate inside the curing part increases even further, it is possible that the sinking effect does not happen. In some situations where the heating effect is intense and the growth in density is slow, the printed part may even move a bit upwards during the print time; in reality, the density increases gradually as the photo-resin converts. If the reaction-induced generated heat is strong enough and the density rise is not considered during the initial stages, there is a chance that the curing part follows an upward trend, provided that the coefficient of thermal expansion would not be small. The upward and downward movement of the printed part can be controlled by adjusting the viscosity of the resin.

Conclusion

****

In this study, a new hypothesis for the different sedimentation behaviors that were reported from different experimental studies in the literature was put forward and investigated numerically. Discrepancies between the experimental results and the results of the previous models were attributed to the heating effects and its effects on mechanical properties, especially density. A CFD model which took advantage of the simplicity of the Boussinesq approximation was developed to numerically investigate the printed part sedimentation in the presence of a heat source. The results show that the heat generated from the exothermic photopolymerization reactions can influence the sedimentation of the part.

Acknowledgement

****

The authors would like to acknowledge the support of the Danish Council for Independent Research (DFF) (Contract No. 0171-00115B).

References

****

[1] B. Kelly, I. Bhattacharya, M. Shusteff, R.M. Panas, H.K. Taylor, C.M. Spadaccini, Computed Axial Lithography (CAL): Toward Single Step 3D Printing of Arbitrary Geometries, (2017). http://arxiv.org/abs/1705.05893.

[2] B.E. Kelly, I. Bhattacharya, H. Heidari, M. Shusteff, C.M. Spadaccini, H.K. Taylor, Volumetric additive manufacturing via tomographic reconstruction, Science (80-.). 363 (2019) 1075–1079. https://doi.org/10.1126/science.aau7114.

[3] D. Loterie, P. Delrot, C. Moser, Volumetric 3D printing of elastomers by tomographic back-projections, Res. Gate. (2018) 1–11. https://doi.org/10.13140/RG.2.2.20027.46889.

[4] D. Loterie, P. Delrot, C. Moser, High-resolution tomographic volumetric additive manufacturing, Nat. Commun. 11 (2020) 1–6. https://doi.org/10.1038/s41467-020-14630-4.

[5] A. Orth, K.L. Sampson, K. Ting, J. Boisvert, C. Paquet, Correcting ray distortion in tomographic additive manufacturing, Opt. Express. 29 (2021) 11037. https://doi.org/10.1364/oe.419795.

[6] C.M. Rackson, J.T. Toombs, M.P. De Beer, C.C. Cook, M. Shusteff, H.K. Taylor, R.R. McLeod, Latent image volumetric additive manufacturing, Opt. Lett. 47 (2022) 1279. https://doi.org/10.1364/ol.449220.

[7] C.M. Rackson, K.M. Champley, J.T. Toombs, E.J. Fong, V. Bansal, H.K. Taylor, M. Shusteff, R.R. McLeod, Object-space optimization of tomographic reconstructions for additive manufacturing, Addit. Manuf. 48 (2021). https://doi.org/10.1016/j.addma.2021.102367.

[8] B. Wang, E. Engay, P.R. Stubbe, S.Z. Moghaddam, E. Thormann, K. Almdal, A. Islam, Y. Yang, Stiffness control in dual color tomographic volumetric 3D printing, Nat. Commun. 13 (2022). https://doi.org/10.1038/s41467-022-28013-4.

[9] C.C. Cook, E.J. Fong, J.J. Schwartz, D.H. Porcincula, A.C. Kaczmarek, J.S. Oakdale, B.D. Moran, K.M. Champley, C.M. Rackson, A. Muralidharan, R.R. McLeod, M. Shusteff, Highly Tunable Thiol-Ene Photoresins for Volumetric Additive Manufacturing, Adv. Mater. 32 (2020) 1–6. https://doi.org/10.1002/adma.202003376.

[10] M. Kollep, G. Konstantinou, J. Madrid-Wolff, A. Boniface, L. Hagelüken, P.V.W. Sasikumar, G. Blugan, P. Delrot, D. Loterie, J. Brugger, C. Moser, Tomographic Volumetric Additive Manufacturing of Silicon Oxycarbide Ceramics, Adv. Eng. Mater. 2101345 (2022). https://doi.org/10.1002/adem.202101345.

[11] J. Madrid-Wolff, A. Boniface, D. Loterie, P. Delrot, C. Moser, Light-based Volumetric Additive Manufacturing in Scattering Resins, (2021) 1–31. http://arxiv.org/abs/2105.14952.
[12] C.M. Rackson, J.T. Toombs, M.P. De Beer, C.C. Cook, M. Shusteff, H.K. Taylor, R.R. McLeod, SinkVsNot.mp4, 2022. https://doi.org/https://doi.org/10.6084/m9.figshare.17064590.v1.
[13] M. Bayat, V.K. Nadimpalli, D.B. Pedersen, J.H. Hattel, A fundamental investigation of thermo-capillarity in laser powder bed fusion of metals and alloys, Int. J. Heat Mass Transf. 166 (2021) 120766. https://doi.org/10.1016/j.ijheatmasstransfer.2020.120766.
[14] M. Bayat, V.K. Nadimpalli, F.G. Biondani, S. Jafarzadeh, J. Thorborg, N.S. Tiedje, G. Bissacco, D.B. Pedersen, J.H. Hattel, On the role of the powder stream on the heat and fluid flow conditions during Directed Energy Deposition of maraging steel—Multiphysics modeling and experimental validation, Addit. Manuf. 43 (2021) 102021. https://doi.org/10.1016/j.addma.2021.102021.
[15] M. Bayat, W. Dong, J. Thorborg, A.C. To, J.H. Hattel, A review of multi-scale and multi-physics simulations of metal additive manufacturing processes with focus on modeling strategies, Addit. Manuf. 47 (2021) 102278. https://doi.org/10.1016/j.addma.2021.102278.
[16] M.P. Serdeczny, R. Comminal, D.B. Pedersen, J. Spangenberg, Numerical prediction of the porosity of parts fabricated with fused deposition modeling, Solid Free. Fabr. 2018 Proc. 29th Annu. Int. Solid Free. Fabr. Symp. - An Addit. Manuf. Conf. SFF 2018. (2020) 1849–1854.
[17] R. Comminal, J.H. Hattel, J. Spangenberg, Numerical Simulations of Planar Extrusion and Fused Filament Fabrication of Non-Newtonian Fluids, Annu. Trans. Nord. Rheol. Soc. (2017). https://nrs.blob.core.windows.net/pdfs/nrspdf-5d42483a-2eeb-43ec-b4ab-a1614ac62f1a.pdf.
[18] M.T. Mollah, R. Comminal, M.P. Serdeczny, D.B. Pedersen, J. Spangenberg, Stability and deformations of deposited layers in material extrusion additive manufacturing, Addit. Manuf. 46 (2021). https://doi.org/10.1016/j.addma.2021.102193.
[19] M.P. Serdeczny, R. Comminal, D.B. Pedersen, J. Spangenberg, Experimental validation of a numerical model for the strand shape in material extrusion additive manufacturing, Addit. Manuf. 24 (2018) 145–153. https://doi.org/10.1016/j.addma.2018.09.022.
[20] R. Comminal, M.P. Serdeczny, D.B. Pedersen, J. Spangenberg, Numerical modeling of the strand deposition flow in extrusion-based additive manufacturing, Addit. Manuf. 20 (2018) 68–76. https://doi.org/10.1016/j.addma.2017.12.013.
[21] R. Salajeghe, M.S. Saidi, Investigation of the different parameters contributing to bubble sticking inside physiological bifurcations, Med. Biol. Eng. Comput. 60 (2022) 599–618. https://doi.org/10.1007/s11517-021-02485-w.
[22] E. Berberović, N.P. Van Hinsberg, S. Jakirlić, I. V. Roisman, C. Tropea, Drop impact onto a liquid layer of finite thickness: Dynamics of the cavity evolution, Phys. Rev. E - Stat. Nonlinear, Soft Matter Phys. 79 (2009). https://doi.org/10.1103/PhysRevE.79.036306.
[23] Y. Tang, STEREOLITHOGRAPHY CURE PROCESS MODELING, Georgia Institute of Technology, 2005. https://www.proquest.com/openview/6457e205c1c9badfde46c992d89ce126/1?cbl=18750&diss=y&pq-origsite=gscholar&parentSessionId=faICL5J9bTengUTJZTMjLjPTfFKBZaj6wSiIUQUsWSo%3D.